Article

The Outer Halos of Very Massive Galaxies: BCGs and their DSC in the Magneticum Simulations

Rhea-Silvia Remus [1],*, Klaus Dolag[1,2], and Tadziu L. Hoffmann[1]

[1]   Universitäts-Sternwarte München, Scheinerstr. 1, D-81679 München, Germany
[2]   Max Planck Institut for Astrophysics, D-85748 Garching, Germany
*   rhea@usm.lmu.de

Abstract: Recent hydrodynamic cosmological simulations cover volumes up to Gpc^3 and resolve halos across a wide range of masses and environments, from massive galaxy clusters down to normal galaxies, while following a large variety of physical processes (star-formation, chemical enrichment, AGN feedback) to allow a selfconsistent comparison to observations at multiple wavelengths. Using the Magneticum simulations we investigate the buildup of the diffuse stellar component (DSC) around massive galaxies within group and cluster environments. The DSC in our simulations reproduces the spatial distribution of the observed intracluster light (ICL) as well as its kinematic properties remarkably well. For galaxy clusters and groups we find that, although the DSC in almost all cases shows a clear separation from the brightest cluster galaxy (BCG) with regard to its *dynamic* state, the radial stellar *density* distribution in many halos is often characterized by a single Sérsic profile, representing both the BCG component and the DSC, very much in agreement with current observational results. Interestingly, even in those halos that clearly show two components in both the dynamics and the spatial distribution of the stellar component, no correlation between them is evident.

Keywords: Galaxy clusters – intracluster light – numerical simulation

1. Introduction

Brightest cluster galaxies (BCGs), residing in the centers of galaxy clusters, are the most massive and luminous galaxies in the universe. During their lifetime they experience frequent interactions with satellite galaxies, and their growth is dominated by merger events. These merger events also lead to the buildup of a diffuse stellar component (DSC), which very likely contains a significant fraction of the total stellar mass of the galaxy clusters (see Murante et al., 2007 [1] and references therein). The velocities of the stars in the BCG and the DSC have distinct kinematic distributions, which can be characterized by two superposed Maxwellian distributions, as demonstrated by Dolag et al., 2010 [2]. While the velocity dispersion of the stars in the BCG represents the central mass of the stars, the velocity dispersion of the DSC is much larger and is comparable to that of the dark matter halo (see, for example, Dolag et al., 2010 [2], Bender et al., 2015 [3], and Longobardi et al., 2015 [4]). More details on this matter can also be found in a recent review by Mihos et al., 2016 [5].

Similarly, early simulations of galaxy clusters found that the density distributions of BCGs in clusters can be described by a superposition of two extended components as well (e.g., Puchwein et al., 2010 [6]). However, more recent simulations find the opposite, namely that in many cases the radial density profiles can be described by a single profile, which is in good agreement with observations. These simulations also indicate that a double-component fit to the radial density profiles is only needed in rare cases. Interestingly, the three-dimensional distribution of these outer stellar halos seems to be

described universally by a so-called Einasto profile over a wide range of halo masses, as shown by Remus et al., 2016 [7], where the curvature of the radial profiles appears to be more closely linked to the cluster's assembly history than the separation of the radial profiles into distinct components.

In this study we analyse the velocity distributions as well as the projected radial surface density profiles of the stellar component in galaxy clusters selected from a state-of-the-art cosmological simulation, and test for possible correlations between these distributions.

2. Simulations

We use galaxy clusters selected from the Magneticum[1] Pathfinder simulation set. This suite of fully hydrodynamic cosmological simulations comprises a broad range of simulated volumes, with box lengths of 2688 Mpc/h to 18 Mpc/h, covering different resolution levels of stellar particle masses from $m_{Star} = 6.5 \times 10^8 M_\odot/h$ at the lowest resolution level down to particle masses of $m_{Star} = 1.9 \times 10^6 M_\odot/h$ at the highest resolution level. For this work we use two different simulations, Box2b and Box4, with the smaller one (Box4) having a higher resolution. The details of these two simulations are summarized in Table 1.

Table 1. Magneticum simulations used in this work.

	box size	N_{part}	m_{Star}	ϵ_{Star}
Box2b hr	910 Mpc	2×2880^3	$3.5 \times 10^7 M_\odot/h$	2 kpc/h
Box4 uhr	68 Mpc	2×576^3	$1.9 \times 10^6 M_\odot/h$	0.7 kpc/h

All simulations of the Magneticum Pathfinder simulation suite are performed with an advanced version of the tree-SPH code P-Gadget3 (Springel, 2005 [8]). They include metal-dependent radiative cooling, heating from a uniform time-dependent ultraviolet background, star formation according to Springel & Hernquist, 2003 [9], and the chemo-energetic evolution of the stellar population as traced by SN Ia, SN II, and AGB stars, including the associated feedback from these stars (Tornatore et al., 2007 [10]). Additionally, they follow the formation and evolution of supermassive black holes, including their associated quasar and radio-mode feedback. For a detailed description see Dolag et al. (in prep), Hirschmann et al., 2014 [11], and Teklu et al., 2015 [12].

Galaxy clusters are chosen according to the total mass of a structure as found by the baryonic SUBFIND algorithm (see Dolag et al., 2009 [13]). For the larger, less resolved volume (Box2b) we classify all structures with masses of $M_{tot} > 2 \times 10^{14} M_\odot$ as clusters, independent of their dynamical state, and find 890 objects. For the smaller volume (Box4) there are no massive galaxy clusters, but the increased resolution enables us to utilize halos with masses down to $1 \times 10^{13} M_\odot < M_{tot} < 1 \times 10^{14} M_\odot$, and therefore allows us to add galaxy groups down to the limit of massive field galaxies to this study. Including the 3 clusters and 35 groups from the smaller volume simulation we end up with a total sample of 928 objects, which is an unprecedentedly large sample of simulated galaxy clusters and groups for which we here, for the first time, provide a statistically representative analysis of the decomposition of the stellar components into the BCG and the DSC, providing predictions for future observational studies of the ICL and the BCGs.

3. Velocity Distributions and Radial Surface Density Profiles

In their detailed study, Dolag et al., 2010 [2] demonstrated that the two dynamical components found in the velocity distribution of the stellar component of galaxy clusters very well represent the stellar component of the BCGs and the DSC, the latter of which is itself a good approximation of the observed ICL in galaxy clusters. Following their approach we subtract all substructures (identified with

---

[1]   www.magneticum.org

SUBFIND) from the stellar component of each cluster and use the remaining stars for this analysis. First, we calculate the velocities of all stellar particles in a cluster and bin them in small equal-width bins of $\Delta v = 10$ km/s, thereby obtaining the intrinsic 3D velocity distribution of the stars in each cluster. Similarly, we choose a random viewing angle and calculate the projected radius of each stellar particle. Subsequently, we radially bin these particles using equal-particle bins, thus obtaining radial surface density distributions, effectively mimicking the radial surface brightness profiles that are commonly observed for galaxies and galaxy clusters, assuming a constant mass-to-light ratio. Examples of the velocity distributions and surface density profiles obtained by this methods are shown in the lower panels of Figures 1, 2, 3, and 4.

To obtain the different components of BCG and DSC in the simulations, we again follow Dolag et al., 2010 [2]. First, we fit a superposition of two Maxwellian distributions

$$N(v) = k_1 v^2 \exp\left(-\frac{v^2}{\sigma_1^2}\right) + k_2 v^2 \exp\left(-\frac{v^2}{\sigma_2^2}\right) \tag{1}$$

to the velocity distribution of each cluster. Additionally, we fit a single Maxwellian distribution to the velocity distributions for comparison purposes. In most cases, a double-Maxwellian fit is needed to properly represent the underlying velocity distributions, as shown, for example, in the lower left panels of Figures 1 and 2. For comparison, we also show the stellar particle surface density map of the clusters including all substructures in the large image at the top of these figures. The white contours show equal-density lines of the stellar distribution without the substructures. For both clusters shown in Figs. 1 and 2, the BCG is clearly visible, but while the velocity distributions can be well described by double-Maxwellian fits in both cases, the morphological appearance of the two clusters is very different: While the cluster shown in Fig. 1 is clearly elongated with a massive colliding structure clearly visible even in the dark matter component (upper small image), the other cluster shown in Fig. 2 shows no signs of ongoing substantial accretion, and is only slightly elongated. This is true even in the X-ray map (middle small image), where the elongation is clearly visible for the first cluster while the second cluster shows a more compact shape. We also do not find a similarity between these clusters with regard to their shock properties: whereas the cluster shown in Fig. 1 has a clearly visible shock front in the upper right area of the cluster, indicating a recent merging event, the cluster shown in Fig. 2 shows no clear signs of such a recent merger event in the shock map (bottom small image). This clearly indicates that the velocity distribution of the cluster remembers the merger history of the cluster over a much larger timescale than other tracers like shocks or satellite distributions, which provide information only about the more recent mass assembly history of a cluster.

In some cases, there is no improvement to the description of the velocity distribution of an individual cluster by using a double-Maxwellian distribution for the fit, as the velocity distributions of that particular cluster is already well described by a single Maxwellian distribution (see, for example, the lower left panel of Fig. 3). While the single-Maxwellian fit is a good approximation to the velocity distribution of the cluster stellar light, the stellar light map in the large image in the same figure clearly shows that the cluster is currently accreting another, relatively massive, substructure. This can be seen not only in the stellar component but also in the X-ray emission (middle small image) and the shock map (bottom small image). Thus, this clearly shows that the contribution from this merger to the cluster's DSC is not very large yet and does not show up in the velocity distribution of the cluster as most stars that are brought in through the merger event have been subtracted by SUBFIND. Only in the very-high velocity end of the velocity distribution, the newly accreted component starts to be visible. This also indicates that the DSC of this cluster is very rich, which is caused by a rather diverse accretion history. However, these cases are very rare as we will show later on in this work.

The lower left panel of Fig. 4 shows a very interesting albeit rare case for the velocity distribution of a galaxy cluster: for this cluster, a double-Maxwellian fit is still not sufficient and a third superposed component would be needed to actually capture all features visible in the velocity distribution.
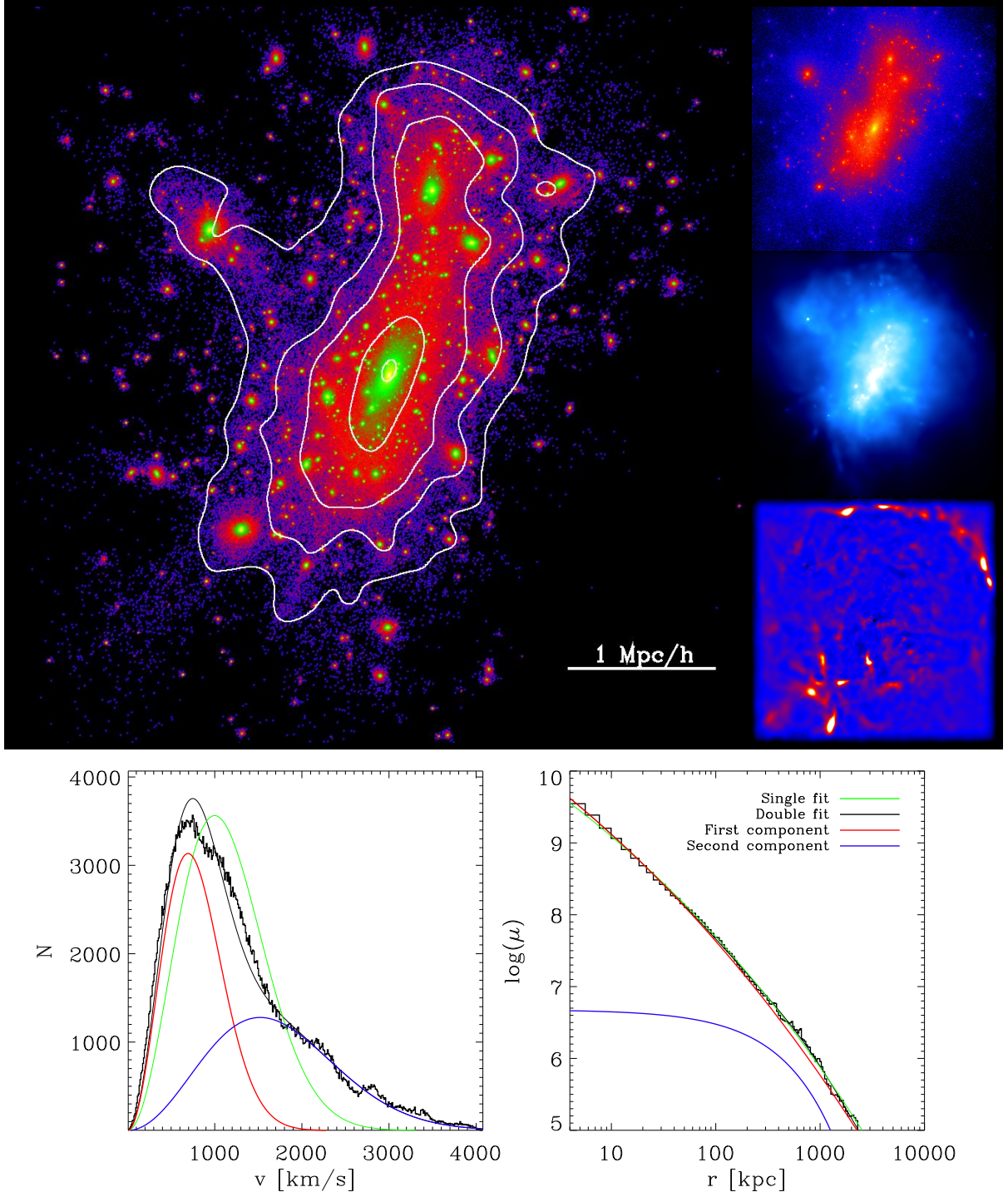
Figure 1. Example of a galaxy cluster where the velocity distribution is best described by a double Maxwellian fit, while the radial surface density profile can be well described by a single Sérsic profile (class d/s). *Upper left panel:* Stellar particle density map of the cluster, with densest areas in yellow/green and least dense areas in blue/black. White contours mark the iso-brightness lines of the DSC with the galaxies subtracted. *Upper right panels, from top to bottom:* Total matter density map; X-ray surface brightness map; unsharp-masked image of the pressure map to visualize shock fronts, as indicated by the large, arc-like feature in the upper right corner. *Lower left panel:* Velocity histogram for the stellar particles within the cluster, excluding those from substructures.   *(Continued in Fig.2.)*
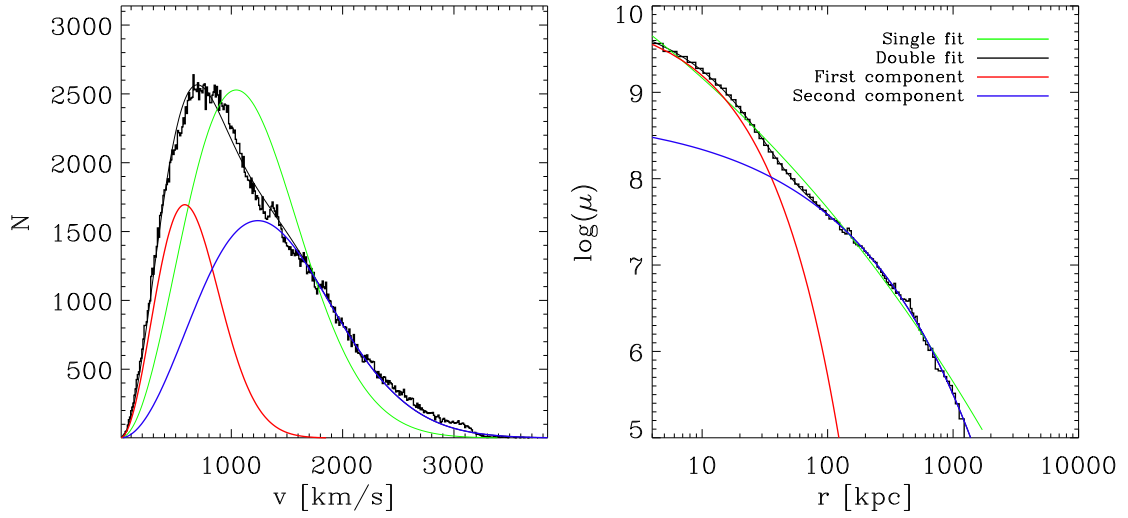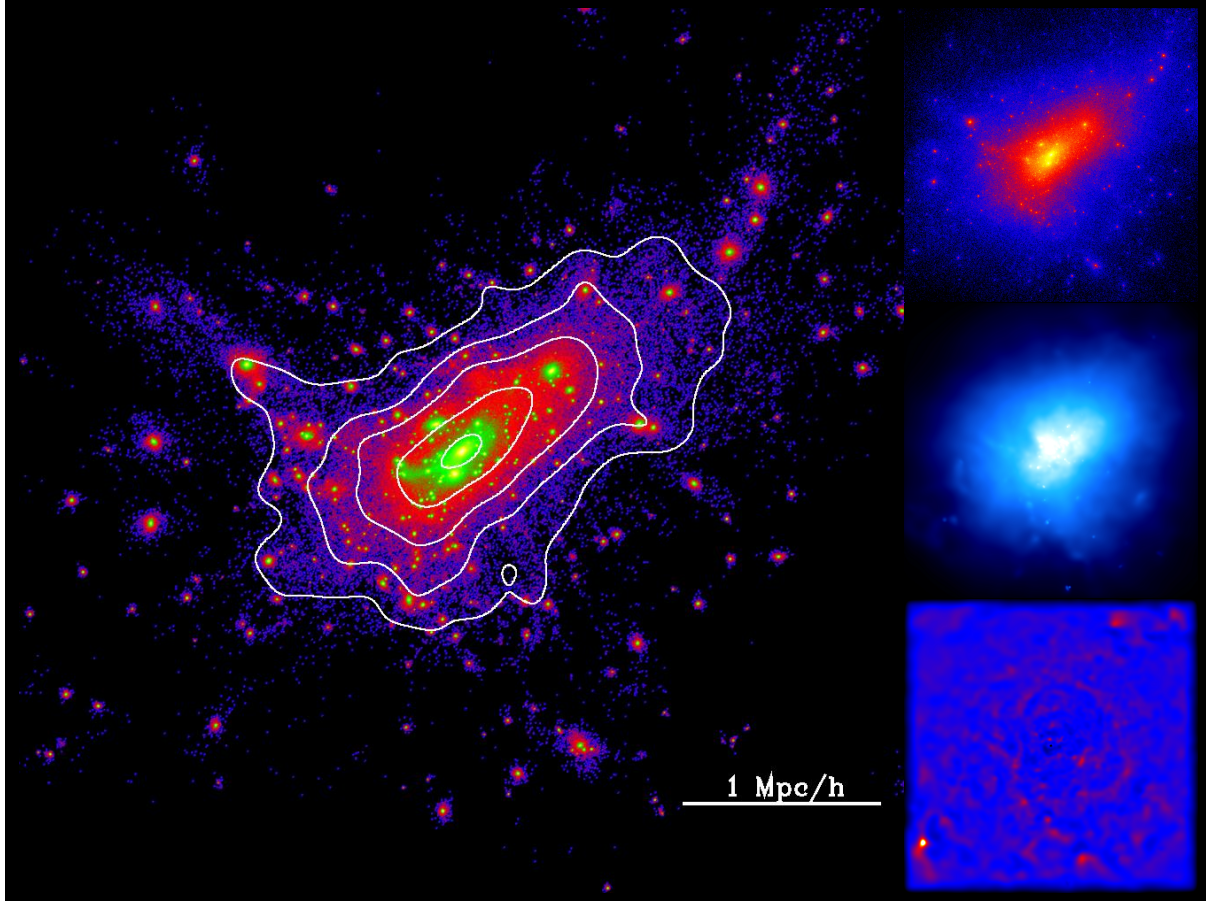
Figure 2. Same as Fig. 1 but for a cluster with a double Maxwellian distribution in the velocity and a double Sérsic radial surface density profile as best representation (class d/d). Although the cluster is quite extended, there are no shocks visible, indicating a very late state of the merger.

(Continued from Fig. 1.) The green line shows the best single-Maxwell fit to the histogram, while the black line shows the best double-Maxwell fit to the histogram with the red and blue lines indicating the individual Maxwellians of the BCG (first) component and the DSC (second) component, respectively. *Lower right panel:* Projected radial stellar surface density profile (with substructures already subtracted) of the cluster centered around the BCG. Colours as in the left panel but for the Sérsic fits.
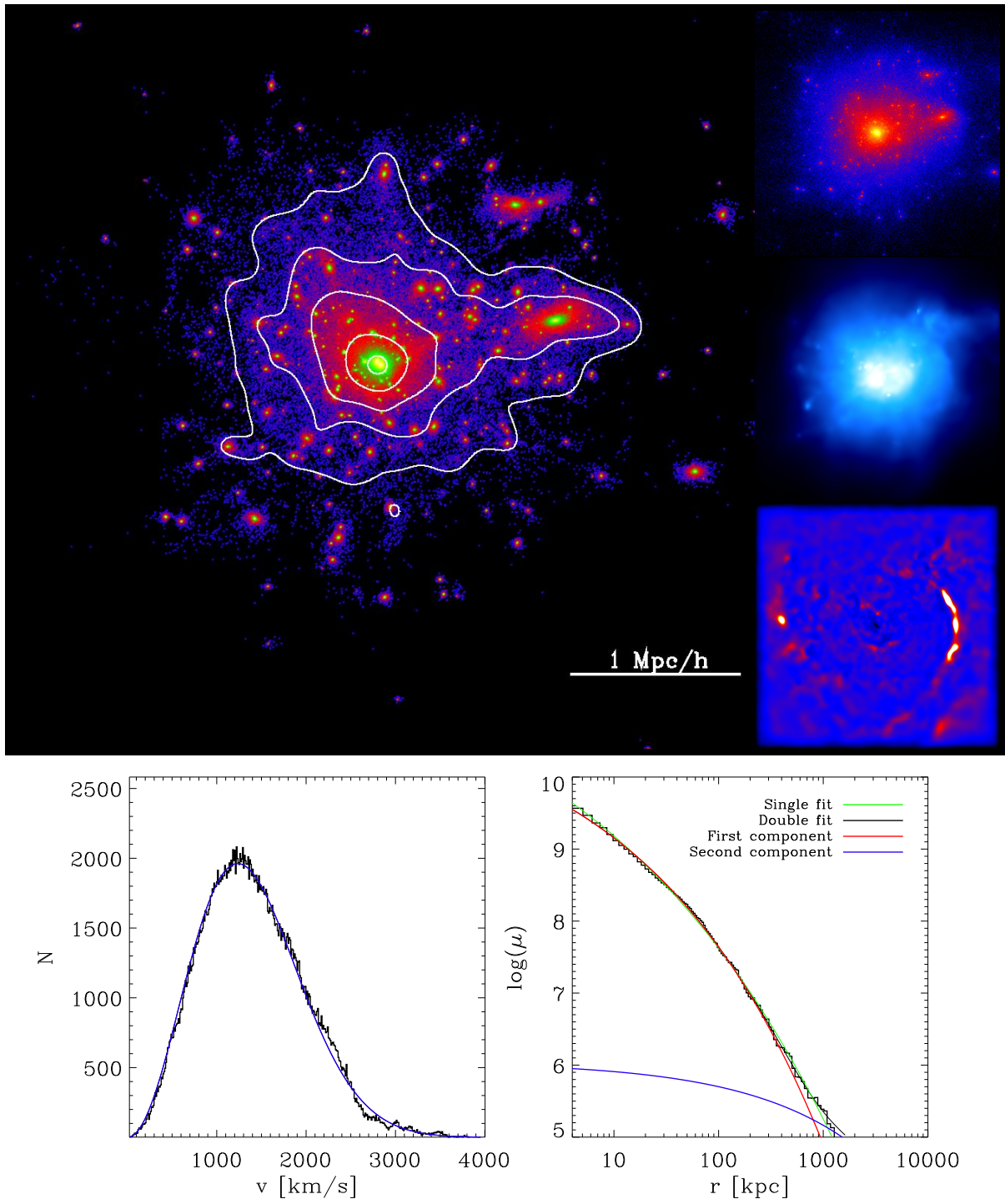
Figure 3. Same as Fig. 1 but for a cluster where the velocity distribution is well described by a single Maxwellian and the radial surface density profile is also well described by a single Sérsic profile (class s/s). Although the outwards-moving substructure to the right has lost all its gas component, the injected shock within the ICM is still clearly visible as a large arc.
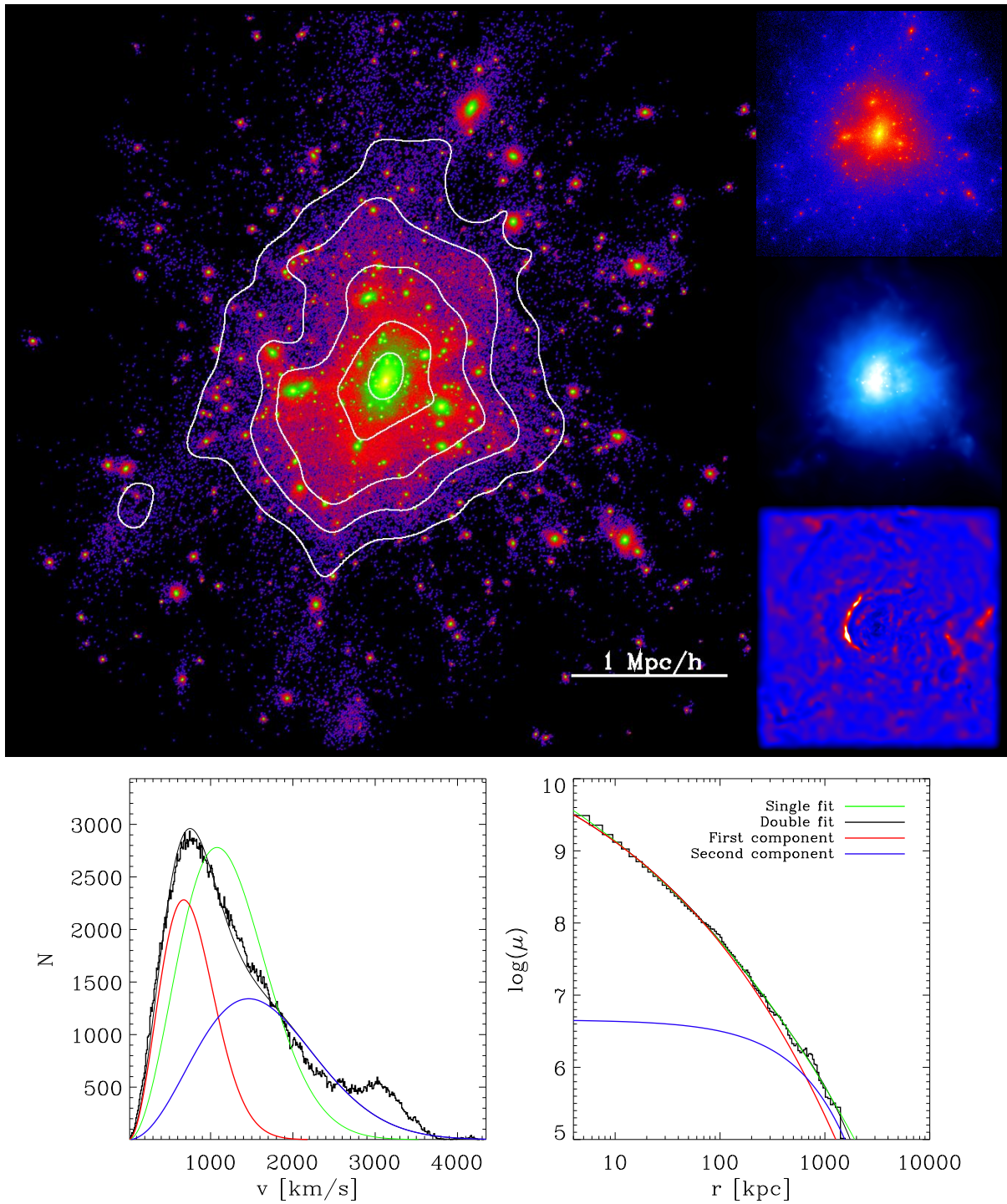
Figure 4. Same as Fig. 1 but for a special case where a third component would be needed to describe the velocity distribution, while the radial surface density profile does not show signs of a third component. Since we do not explicitly study these special cases in this work, this cluster is classified as belonging belong to the d/d class, as both the velocity and the radial density clearly are multi-component systems.
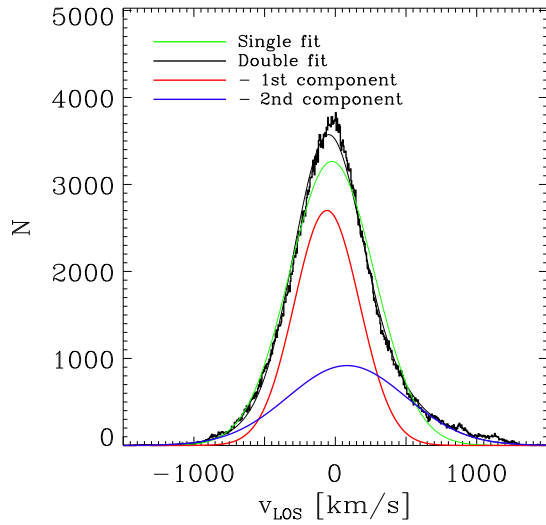
Figure 5. Line-of-sight velocity distributions of the stellar particles (excluding those bound to substructures) of the cluster shown in Fig. 1, from a random projection. The green line is the best single Gaussian fit to the distribution, while the black line is the best double-Gaussian fit with its components shown in red and blue.

116 Interestingly, this new accretion is not strongly visible in the maps in the upper panels of this figure. The
117 stellar component of the merger ongoing in the central part of the cluster – clearly visible through the
118 displacement of the central X-ray emission from the centre of mass towards the left as well as through
119 the clearly visible shock moving from the centre leftwards – is most likely the third, high velocity
120 component in the velocity distribution. As these cases are rare and need a visual inspection of all 928
121 clusters to identify them, we will not introduce these objects as a separate class of velocity distributions
122 in this work, and will here simply classify them as double-Maxwellian velocity distributions.

123 While in this three dimensional analysis the two different velocity components of the BCG and
124 the DSC are nicely visible, this information cannot be drawn directly from observations. However,
125 observationally the line-of-sight velocity can be measured and used as a substitute to distinguish the
126 two components: In projection, the measured velocity is not represented by a Maxwellian distribution
127 but by a Gaussian distribution, an example of which is shown in Fig. 5, where we plot the line-of-sight
128 velocity distribution of the cluster shown in Fig. 1. As for the three dimensional case, also in the
129 projected case a superposition of two Gaussian fits is needed to represent the velocity distribution
130 profile, clearly indicating the two-component structure of the BCG and the DSC. In case of an ideal
131 spherically symmetric relaxed system the projected Gaussian fits predict the same mass fractions and
132 velocity dispersions for the BCG component and the DSC as the intrinsic Maxwellian distribution fits,
133 but projection effects, asymmetries as well as distortion effects through accretion events can lead to
134 (slightly) different values. However, we do not investigate these issues further in this work.

For the radial surface density profiles, we use a similar approach as for the velocity distributions. We fit the superposition of two Sérsic profiles

$$\mu(r) = \mu_1 \exp\left(-\left(\frac{r}{r_1}\right)^{1/n_1}\right) + \mu_2 \exp\left(-\left(\frac{r}{r_2}\right)^{1/n_2}\right) \tag{2}$$

135 to the radial surface density profiles of each cluster, and for comparison we also fit a single Sérsic
136 profile as well.

137 Examples for the resulting Sérsic fits to the surface density distributions are shown in the lower
138 right panels of Figures 1, 2, 3, and 4. As for the velocity distributions, we also see that there is no clear
139 correlation between the visual appearance of the clusters, neither in the stellar nor the X-ray or the
140 shock appearance, and the necessity of a double-Sérsic fit. Interestingly, we can already see from these
141 four examples that there is also no clear correlation between the presence of a second component in the
142 velocity distribution and the presence of a second component in the radial density profile: as shown
143 in Fig. 1, there are clusters that display two components in the velocity distribution but only a single
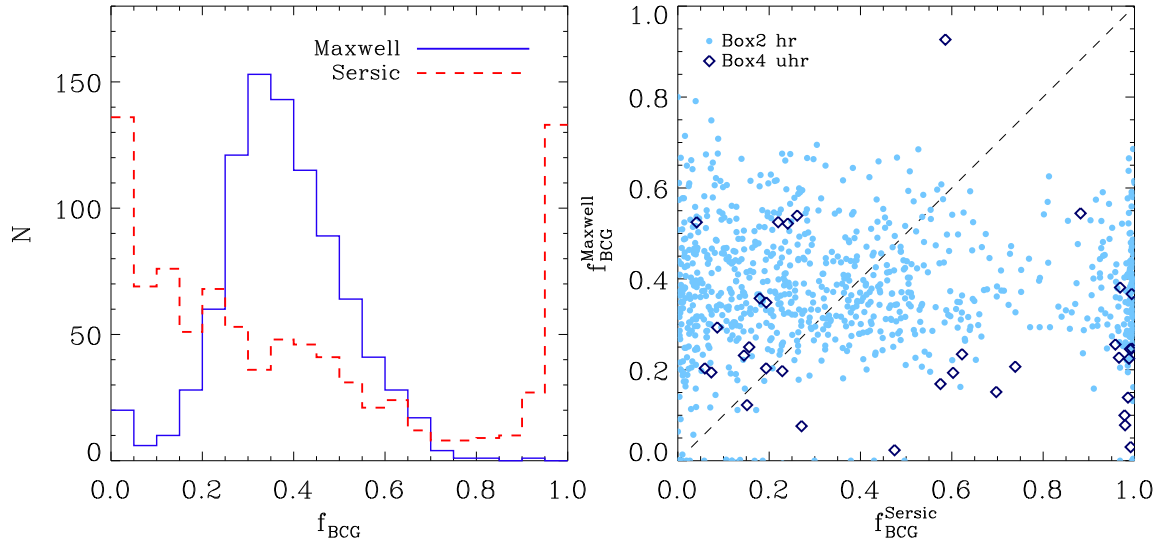
Figure 6. *Left panel:* Histogram of the mass fraction ascribed to the BCG according to the double-Maxwell fits (blue) and the double-Sérsic fits (red). The mass ascribed to the BCG is always the mass of the slower (Maxwellian fits) or the innermost (Sérsic fits) component. *Right panel:* BCG mass fractions obtained from the Maxwell fits versus that obtained with the Sérsic fits. Light blue symbols show the clusters from Box2b, while dark blue open diamonds mark the galaxy groups selected from Box4. There is no evident correlation between the mass partitioning obtained with the two different methods, and there is also no difference between galaxy groups and clusters.

component in the radial surface density profile, while Fig. 2 shows a cluster where both distributions have a double structure. In the following we will study this behaviour in more detail.

3.1. Statistical properties

As we cannot check the properties of all 928 galaxy clusters from our sample individually, we now try to quantify their behaviour in a more statistical way. The biggest issue here is that a double fit with twice as many free parameters as a single fit will always yield a better fit, or one at least as good, according to simple statistical tests like χ^2 or Komolgorov-Smirnov, if the number of degrees of freedom is much larger than the number of fit parameters (as is the case here). Thus, we need to find a better way to decide which fit adequately characterizes the properties in velocity and surface brightness of a cluster.

One way to do this is to use the double-Maxwell and double-Sérsic fits of a cluster and integrate over each of the two components. This way, assuming that the two components always represent an inner, slower component that describes the BCG and an outer, faster component that describes the DSC, we can obtain the fraction of mass associated with each component, relative to the total stellar mass given by the full velocity distribution and the full radial surface density profile.

The left panel of Fig. 6 shows a histogram of the mass fractions of the BCG, f_{BCG}, obtained with both methods for all 928 halos. The blue line shows the distribution found from the double-Maxwell fits, while the red line shows the fractions obtained from the double-Sérsic fits. The right panel of the same figure shows a scatter plot of the BCG mass fractions obtained with both methods. As can clearly be seen there is no correlation at all between the mass fractions resulting from the two methods: while there is only a small amount of clusters that have BCG mass fractions below 10% and none with BCG mass fractions above 90% according to the double-Maxwell method, the double-Sérsic method results in about half of the clusters having BCG mass fractions of about 0% or 100%, clearly indicating that

Table 2. Relative fractions of the 928 clusters and groups with regard to their Maxwell- and Sérsic-fit properties.

	$N_{cluster}$	$f_{cluster}(\%)$
Single Maxwell sufficient	53	5.7
Double Maxwell needed	875	94.3
Single Sérsic sufficient	386	41.6
Double Sérsic needed	542	58.4
Single Maxwell, Single Sérsic (s/s)	29	3.1
Double Maxwell, Single Sérsic (d/s)	357	38.5
Single Maxwell, Double Sérsic (s/d)	24	2.6
Double Maxwell, Double Sérsic (d/d)	518	55.8

167 in those cases a double-Sérsic fit is not necessary and their radial surface density profiles can be well
168 described by a single Sérsic profile.

169 The latter is in good agreement with observations of radial surface brightness profiles for massive
170 elliptical galaxies, where both single- and double-Sérsic-profiles are observed without a clear correlation
171 to the global dynamical state of the cluster. From the double-Maxwell method, we find BCG mass
172 fractions generally ranging between $20\% < f_{BCG} < 70\%$, but the large mass fractions are rare and
173 most of the BCGs have mass fractions between 30 and 40%, which is in agreement with observational
174 fractions obtained for the BCGs in very massive clusters (e.g., Presotto et al., 2014 [14], Burke et al.,
175 2015 [15]).

176 We use the BCG mass fractions obtained with both methods to decide whether a double-
177 component fit is needed for the velocity distributions and the surface density profiles or if a single-
178 component fit is sufficient: if the BCG mass fraction obtained through a double-Maxwell fit is below
179 $f_{BCG} = 10\%$ or above $f_{BCG} = 90\%$, we judge that there is no clear signal of a second component
180 in this fit and we thus classify these clusters as single-Maxwell clusters. If the BCG mass fraction
181 is between these values, i.e., $10\% < f_{BCG} < 90\%$, we gauge the double-Maxwell-fit to be necessary
182 and thus classify the cluster as double-Maxwell cluster. As shown in the upper part of Table 2, the
183 fraction of single-Maxwell clusters is below 6%, and nearly all clusters show velocity distributions
184 that reflect two-component systems. Therefore, we conclude that the typical galaxy cluster shows
185 a two-component behaviour in its velocity distribution, in agreement with recent observations, for
186 example, by Longobardi et al., 2015 [4] and Bender et al., 2015 [3].

187 Similarly, we classify a galaxy cluster as single-Sérsic cluster if the BCG mass fraction obtained
188 from the double-Sérsic fit is below $f_{BCG} = 10\%$ or above $f_{BCG} = 90\%$, while we classify a cluster as
189 double-Sérsic cluster if the BCG mass fraction is between $10\% < f_{BCG} < 90\%$. Here, we clearly see
190 the same split-up that we already saw from Fig. 6, i.e., that about half of the clusters are single-Sérsic
191 clusters while the other half are double-Sérsic clusters, with a slight trend towards the latter (see upper
192 part of Table 2).

193 Using both classifications we can now test how many clusters show a double-fit-behaviour in
194 both the velocity distribution and the surface density profiles. We find that this is the case for more
195 than half of the galaxy clusters in our sample, as shown in the lower part of Table 2 and Fig. 7, while
196 about 40% of the clusters are double-Maxwell but single-Sérsic clusters. The single-Maxwell clusters
197 represent less than 6% of all our clusters; they are roughly evenly distributed between single-Sérsic
198 and double-Sérsic cases.

199 From these results we conclude that the velocity distribution of a cluster can still distinguish
200 between the component that belongs to the direct potential of the BCG and the outer component
201 that was accreted onto the cluster and stored in the outer regions of the BCG through stripping and
202 flyby events, building up the DSC component that still retains this memory of the assembly history.
203 On the other hand, the imprint of this assembly history is not always visible in the radial surface
204 density profiles of the cluster BCGs as a separate component, where only in some cases the BCG can be
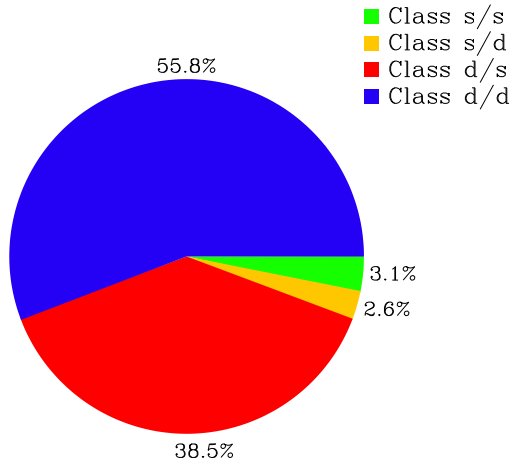
Figure 7. Fraction of galaxy clusters and groups that can be described best by a single Maxwell distribution and a single Sérsic profile (class s/s; green), a double Maxwell distribution and a single Sérsic profile (class d/s; red), a single Maxwell distribution and a double Sérsic profile(class s/d; yellow), and a double Maxwell distribution and a double Sérsic profile (class d/d; blue).

separated from the DSC through the surface density profiles, while in other cases this is not possible. Whether the assembly history can be traced from the shape of the outer stellar halo radial density profiles of BCGs and galaxies in general will be part of a forthcoming study (see Remus et al., 2016 [7] for a preview on these results).

4. Mass–Velocity-Dispersion Relation

Finally, we want to see if a correlation exists between the velocity dispersion obtained from the Maxwell fits for the BCG and the DSC and the virial mass of the host cluster, as presented by Dolag et al., 2010 [2]. For this purpose, the left panel of Fig. 8 shows the velocity dispersion of the BCG component versus the virial mass of the cluster in red, and the velocity dispersion of the DSC versus the virial mass of the cluster in blue. As can clearly be seen, we find a strong correlation for both components with the virial mass of the cluster, and these correlations hold even for the galaxy groups in the lower mass regime, indicating that the split-up between the brightest group galaxies (BGGs) and the Intra-group light (IGL) behaves similarly to that of clusters, clearly hinting at a similar growth mechanism for the IGL through stripping.

The left panel of Fig. 8 also shows the fits to the velocity-dispersion–virial-mass relation presented by Dolag et al., 2010 [2] as red and blue dotted lines for the BCGs and the DSC, respectively. Although not fitted to the current simulation set but obtained from a less advanced simulation set of the local universe, these relations perfectly describe the behaviour found for the Magneticum simulation sample of galaxy clusters and galaxy groups, even at the low mass end. This additionally proves that this behaviour is independent of the details of the subgrid models included in the simulations.

As can also be seen from Fig. 8, the relation between the velocity dispersion and the virial mass for the BCGs and the DSC has the same slope, with the DSC simply having overall larger velocity dispersions than the BCGs. More precisely, as shown in the right panel of Fig. 8, the relation between the velocity dispersions of the BCG and the DSC is very tight and can be described as

$$\sigma_{\text{BCG}} = 0.5\,\sigma_{\text{DSC}}. \tag{3}$$

Again, this behaviour holds even at the galaxy group mass scale, as indicated by the open diamonds marking the groups selected from the smaller volume Box4 with the higher resolution. In addition, this not only demonstrates that galaxy groups and clusters show a similar behaviour, but it also proves that the correlations presented here are independent of the resolution of the simulation and thus only driven by physical processed like accretion and star formation.

Interestingly, we can also explain the few outliers that can be seen in both the velocity-dispersion– virial-mass relation and the velocity-dispersion relation between the BCGs and their DSC: if we mark
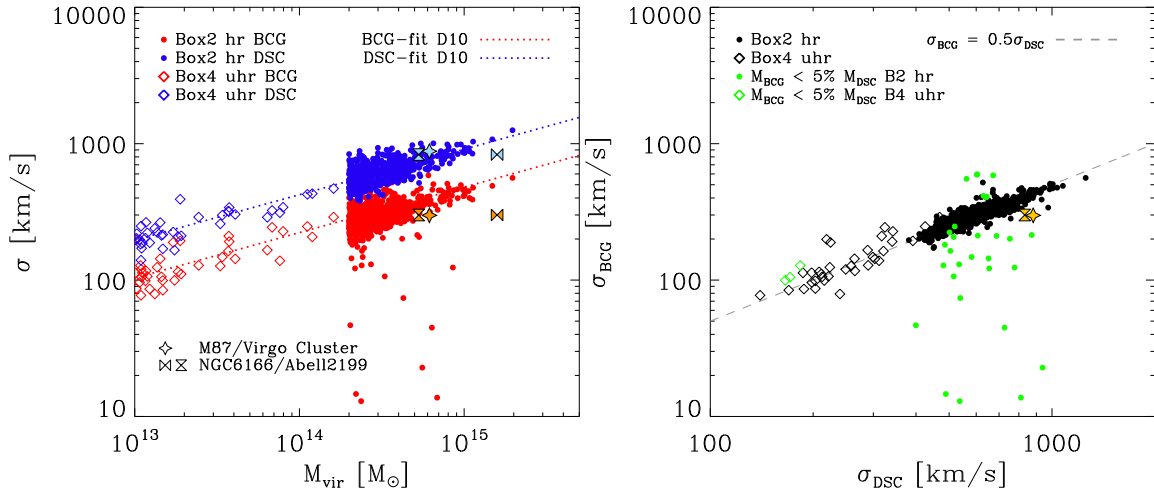
Figure 8. *Left panel:* Velocity dispersion σ obtained from the double-Maxwellian fit versus virial mass M_{vir} for the BCG-component (red) and the DSC-component (blue) for all galaxy clusters in Box2b (filled circles) and all galaxy groups in Box4 (open diamonds). The red and blue lines are not fitted to the data presented here but are those from Dolag et al., 2010 [2]. The orange and light blue symbols show velocity dispersions from observations of NGC 6166 in the cluster Abell 2199 (bowties/hourglases) from Bender et al., 2015 [3] and M 87 in the Virgo cluster (stars) from Longobardi et al., 2015 [4]. The virial mass for Virgo is taken from Tully, 2015 [16] using the average of the masses based on the total K-band luminosity and the virial mass inferred from the zero velocity surface. For Virgo this is in agreement with measurements by PLANCK [17], for Abell 2199 we included measurements of the virial mass from the PLANCK mission [17] (hourglasses) as they give significantly smaller values than the one inferred by Tully (2015) [16] (bowties). *Right panel:* BCG velocity dispersion σ_{BCG} versus DSC velocity dispersion σ_{DSC} obtained from the double-Maxwellian fits for the same clusters (filled circles) and groups (open diamonds) as in the left panel. The grey dashed line shows the $\sigma_{\mathrm{BCG}} = 0.5\,\sigma_{\mathrm{DSC}}$ relation. Green symbols mark all clusters and groups for which the BCG-component has less than 5% of the stellar mass of the total stellar mass of the system, according to the mass partitioning obtained from the double-Maxwellian fit. The yellow symbols show the same observations as in the left panel.

all clusters (and groups) where the BCG mass fraction obtained from the double-Maxwellian fit is below 5% (green circles and diamonds in the right panel of Fig. 8), all outliers are captured. This clearly indicates that for all galaxy clusters where a double-Maxwellian fit is the better representation of the velocity distribution, the discussed relation between both components and the virial mass of the cluster is present and very tight, and driven by the assembly history of the clusters.

In addition, we also included the observations for NGC 6166 in the cluster Abell 2199 from Bender et al., 2015 [3] and M 87 in the Virgo cluster from Longobardi et al., 2015 [4] in both panels of Fig. 8 (for details on the virial mass estimated for these clusters see the figure caption). Both observations are in excellent agreement with the correlations found in this study, especially with respect to the BCG–DSC velocity dispersion correlation.

5. Discussion and Conclusion

In this work we presented a detailed and statistically sound analysis of the stellar velocity distributions and the projected stellar radial surface density profiles of galaxy clusters and galaxy groups selected from the Magneticum pathfinder simulation sample. Using two volumes of different sizes and resolutions, we showed that for more than 90% of all 928 clusters and groups in our sample the velocity distributions are represented best by a superposition of two Maxwellian distributions,

with the slower component representing the BCG of the cluster and the faster component representing the DSC. We demonstrated that the relative mass fractions of the BCGs found through these fits is in agreement with recent observations. This behaviour in the velocity distribution strongly supports the idea that the DSC is built up from stripping of smaller satellites within the cluster potential close to its center, where the BCG resides.

Furthermore, we found that there is a clear and tight correlation between the velocity dispersions of the two components obtained by these fits and the virial mass of the host clusters, and that this correlation holds down to group-mass scales. We also demonstrated that the velocity dispersions of both components are correlated tightly, with the BCG having about half the velocity dispersion of the DSC, and that the few available observations that distinguish between both components are in excellent agreement with our results.

Additionally, we tested if the same separation into two distinct components is reflected in the projected radial surface density profiles of the cluster. Interestingly, we could only find a separation of the radial profiles into two components in about half of the clusters that exhibit a double-Maxwell imprint in the velocity distribution, clearly showing that the radial profile is not always suitable for distinguishing the two components and that further indicators are needed in the radial stellar profiles to obtain information about the assembly history of galaxy clusters. This issue will be addressed in a forthcoming study.

Lastly, we also tested if we can find a correlation between the velocity distribution behaviour of the DSC and the X-ray or shock properties in the four objects we have examined in detail. No such correlations were evident. On the contrary, we find indications that the X-ray and shock properties describe the very recent assembly history of the cluster, where the presence of shocks and X-ray offsets indicate an ongoing merger event, while the velocity distribution of the stellar component of the galaxy clusters and the BCGs appears to be an indicator for the earlier assembly history of the cluster.

Author Contributions: K. D. performed the simulations; R.-S. R. and T. L. H. analysed the data; R.-S. R wrote the paper.

Conflicts of Interest: The authors declare no conflict of interest.

References

1. Murante, G.; Giovalli, M.; Gerhard, O.; Arnaboldi, M.; Borgani, S.; Dolag, K. The importance of mergers for the origin of intracluster stars in cosmological simulations of galaxy clusters. *MNRAS* **2007**, *377*, 2–16, [astro-ph/0701925].

2. Dolag, K.; Murante, G.; Borgani, S. Dynamical difference between the cD galaxy and the diffuse, stellar component in simulated galaxy clusters. *MNRAS* **2010**, *405*, 1544–1559, [0911.1129].

3. Bender, R.; Kormendy, J.; Cornell, M.E.; Fisher, D.B. Structure and Formation of cD Galaxies: NGC 6166 in ABELL 2199. *ApJ* **2015**, *807*, 56, [1411.2598].

4. Longobardi, A.; Arnaboldi, M.; Gerhard, O.; Hanuschik, R. The outer regions of the giant Virgo galaxy M 87: Kinematic separation of stellar halo and intracluster light. *A&A* **2015**, *579*, A135, [1502.02032].

5. Mihos, J.C. Intragroup and Intracluster Light. The General Assembly of Galaxy Halos: Structure, Origin and Evolution; Bragaglia, A.; Arnaboldi, M.; Rejkuba, M.; Romano, D., Eds., 2016, Vol. 317, *IAU Symposium*, pp. 27–34, [1510.01929].

6. Puchwein, E.; Springel, V.; Sijacki, D.; Dolag, K. Intracluster stars in simulations with active galactic nucleus feedback. *MNRAS* **2010**, *406*, 936–951, [1001.3018].

7. Remus, R.S.; Burkert, A.; Dolag, K. A "Universal" Density Profile for the Outer Stellar Halos of Galaxies. *ArXiv e-prints* **2016**, [1605.06511].

8. Springel, V. The cosmological simulation code GADGET-2. *MNRAS* **2005**, *364*, 1105–1134.

9. Springel, V.; Hernquist, L. Cosmological smoothed particle hydrodynamics simulations: a hybrid multi-phase model for star formation. *MNRAS* **2003**, *339*, 289–311.

10. Tornatore, L.; Borgani, S.; Dolag, K.; Matteucci, F. Chemical enrichment of galaxy clusters from hydrodynamical simulations. *MNRAS* **2007**, *382*, 1050–1072, [0705.1921].

11. Hirschmann, M.; Dolag, K.; Saro, A.; Bachmann, L.; Borgani, S.; Burkert, A. Cosmological simulations of black hole growth: AGN luminosities and downsizing. *MNRAS* **2014**, *442*, 2304–2324, [1308.0333].

12. Teklu, A.F.; Remus, R.S.; Dolag, K.; Beck, A.M.; Burkert, A.; Schmidt, A.S.; Schulze, F.; Steinborn, L.K. Connecting Angular Momentum and Galactic Dynamics: The Complex Interplay between Spin, Mass, and Morphology. *ApJ* **2015**, *812*, 29, [1503.03501].

13. Dolag, K.; Borgani, S.; Murante, G.; Springel, V. Substructures in hydrodynamical cluster simulations. *MNRAS* **2009**, *399*, 497–514, [0808.3401].

14. Presotto, V.; Girardi, M.; Nonino, M.; Mercurio, A.; Grillo, C.; Rosati, P.; Biviano, A.; Annunziatella, M.; Balestra, I.; Cui, W.; Sartoris, B.; Lemze, D.; Ascaso, B.; Moustakas, J.; Ford, H.; Fritz, A.; Czoske, O.; Ettori, S.; Kuchner, U.; Lombardi, M.; Maier, C.; Medezinski, E.; Molino, A.; Scodeggio, M.; Strazzullo, V.; Tozzi, P.; Ziegler, B.; Bartelmann, M.; Benitez, N.; Bradley, L.; Brescia, M.; Broadhurst, T.; Coe, D.; Donahue, M.; Gobat, R.; Graves, G.; Kelson, D.; Koekemoer, A.; Melchior, P.; Meneghetti, M.; Merten, J.; Moustakas, L.A.; Munari, E.; Postman, M.; Regős, E.; Seitz, S.; Umetsu, K.; Zheng, W.; Zitrin, A. Intracluster light properties in the CLASH-VLT cluster MACS J1206.2-0847. *A&A* **2014**, *565*, A126, [1403.4979].

15. Burke, C.; Hilton, M.; Collins, C. Coevolution of brightest cluster galaxies and intracluster light using CLASH. *MNRAS* **2015**, *449*, 2353–2367, [1503.04321].

16. Tully, R.B. Galaxy Groups: A 2MASS Catalog. *AJ* **2015**, *149*, 171, [1503.03134].

17. Planck Collaboration.; Ade, P.A.R.; Aghanim, N.; Arnaud, M.; Ashdown, M.; Aumont, J.; Baccigalupi, C.; Banday, A.J.; Barreiro, R.B.; Barrena, R.; et al.. Planck 2015 results. XXVII. The second Planck catalogue of Sunyaev-Zeldovich sources. *A&A* **2016**, *594*, A27, [1502.01598].